A non-local Chan-Vese model for sparse, tubular object segmentation

Anna Jezierska, Olivia Miraucourt, Hugues Talbot, Stéphanie Salmon, Nicolas Passat

A NON-LOCAL CHAN-VESE MODEL FOR SPARSE, TUBULAR OBJECT SEGMENTATION

Anna Jezierska[1], *Olivia Miraucourt*[1,2], *Hugues Talbot*[1], *Stéphanie Salmon*[2], *Nicolas Passat*[2]

[1] Université Paris-Est, ESIEE, CNRS, LIGM, France
[2] Université de Reims Champagne-Ardenne, LMR & CReSTIC, France

ABSTRACT

To deal with the issue of tubular object segmentation, we propose a new model involving a non-local fitting term, in the Chan-Vese framework. This model aims at detecting objects whose intensities are not necessarily piecewise constant, or even composed of multiple piecewise constant regions. Our problem formulation exploits object sparsity in the image domain and a local ordering relationship between foreground and background. A continuous optimization scheme can then be efficiently considered in this context. This approach is validated on both synthetic and real retinal images. The non-local data fitting term is shown to be superior to the classical piecewise-constant model, robust to noise and to low contrast.

***Index Terms*—** Variational image segmentation, non-local data fidelity, tubular structures, angiographic imaging.

1. INTRODUCTION

In various kinds of images, some structures of interest appear as thin, tubular objects, i.e., structures that are significantly longer in one dimension compared to the others, and that may be only a few pixel thick or less in places. Such structures also tend to be sparse in the image domain and sensitive to noise. Vascular structures are typical examples. Their reliable segmentation is indeed a challenging task, however crucial for many (bio)medical applications, both in 2D (retinal) [1] and 3D (MRA, CTA) images [2, 3, 4, 5]. In 3D, intensity variations may result from various sources of noise and acquisition artifacts. In 2D, intensity inhomogeneities generally derive from illumination conditions during acquisition.

These difficulties have motivated many contributions, among them extensions to the Chan-Vese model have received specific attention. Chan and Vese proposed an active contour model, dividing an image into two regions based on a minimal variance criterion, such that each region is attributed a single mean intensity value. In particular, the two-phase Chan-Vese model, under the assumption that the two piecewise constant values are known, is a convex problem that can be solved exactly [6, Th. 2].

This research was partially funded by a grant from the *Région Champagne-Ardenne* and by *Agence Nationale de la Recherche* (Grant Agreement ANR-12-MONU-0010).

In the context of sparse, tubular structures with inhomogeneous signal, extensions of the Chan-Vese model have been proposed for both the data fidelity and prior terms. The latter have led to the development of tubularity and connectivity priors, e.g., superellipsoids [7], B-splines framelet [8], adaptive dictionaries [9] and elastic connectivity [10]. The need to be robust to background variability led to the replacement of the global data fidelity term, developed under the piecewise constant assumption, by a compound global-local term [11, 12].

A simplified global model (Sec. 2) was introduced, e.g., in [13, 14, 15, 16, 8]. However, the associated global data fidelity term is not well suited for non-uniform region segmentation problems [17]. Hence, local information was additionnaly exploited, by computing local regional statistics. In [18], a multiple piecewise constant active contour model aims at clustering regions, assigning to each induced subregion a single mean intensity value. The outcome depends on an initial k-means clustering, that requires well contrasted images. In [19] a fuzzy non-local model is proposed, where a vector field is attributed to each region, whose coefficients are calculated as weighted NL-means. This leads to good results, except for low-contrast, due to the sensitivity to the neighbourhood choice. In [20], a data fidelity term built on vector valued similarity between local histograms was introduced. This method, designed for textured image segmentation, is not well suited to the case of thin object segmentation, where foreground signal can be quite sparse. For similar reasons, other internal energy measures [17, 21] are not well suited to the case of sparse objects. In [11], the global Chan-Vese model is combined with a local term built on a local contrast map. This strategy is sensitive to noise with small neighbourhood sizes, while at larger sizes it is less sensitive to noise but loses the finest details.

To overcome these problems, we propose a new model with a non-local fitting term for detecting thin, sparse tubular objects (Sec. 3). This model can detect objects that are not necessarily piecewise constant, or composed of multiple piecewise constant regions. Our problem formulation exploits object sparsity in the image domain and a global ordering relationship between foreground and background. More precisely, this new energy formulation – additionally to some connectivity, regularity or tubularity priors – includes a spar-

sity prior term and a non-local data fidelity term, where each region is attributed a vector field, whose coefficients are calculated as a quantile of a random variable associated with a patch centered in each image pixel. We propose to solve this problem efficiently using a continuous optimization framework (Sec. 4), through the use of convex relaxation techniques [6, 22]. The performance of the proposed approach is illustrated with a 3D synthetic image example containing complex, curvilinear, objects with varying intensities, inhomogeneous background and Gaussian noise. It is also tested on real 2D retinal images (Sec. 5).

2. GENERAL PROBLEM FORMULATION

Let $\mathbb{X}$, $\mathbb{X}_0$, $\mathbb{X}_1$ denote image, background and target signal supports, respectively. We consider the two-phase image segmentation problem, that consists of finding an optimal partition $(\mathbb{X}_0, \mathbb{X}_1)$ of $\mathbb{X}$, based on the observation vector $y \in \mathcal{Y} = \mathbb{R}^N$. Using the auxiliary variable $x \in \mathcal{X} = [0,1]^N$ and threshold $\tau \in [0,1]$ related with sets $\mathbb{X}_0$ and $\mathbb{X}_1$ by

$$\forall i \in \mathbb{X} \begin{cases} i \in \mathbb{X}_0 & \text{if } x_i < \tau \\ i \in \mathbb{X}_1 & \text{otherwise} \end{cases} \tag{1}$$

the problem can be formulated as a minimization problem, aiming at finding

$$\underset{x \in \mathcal{X}}{\operatorname{argmin}}\ f(x) \tag{2}$$

where

$$f(x) = \Phi(x) + \rho(x) + \iota_{\mathcal{X}}(x) \tag{3}$$

The objective function f is defined as a sum of data fidelity term

$$\begin{aligned} \Phi(x) &= \psi_0(x) + \psi_1(x) \qquad (4)\\ &= \sum_{i \in \mathbb{X}} \varphi_0(x_i)\ \phi(y_i - u_i^1) + \sum_{i \in \mathbb{X}} \varphi_1(x_i - 1)\ \phi(y_i - u_i^0) \end{aligned}$$

hybrid regularization term

$$\rho(x) = \sum_{r=2}^{R} \psi_r(V_r x) + \nu\varphi(x) \tag{5}$$

and an indicator function of a convex set $\mathcal{X}$

$$\forall i \in \mathbb{X}, \iota_{\mathcal{X}}(x_i) = \begin{cases} 0 & \text{if } x_i \in [0,1] \\ +\infty & \text{otherwise} \end{cases} \tag{6}$$

where $R \in \mathbb{N}$, $R \geq 2$; $\nu \in \mathbb{R}^+$; for all $r = \{2, \ldots, R\}$, $V_r : \mathcal{X} \mapsto \mathbb{R}^{P_r}$ is a linear operator; ψ_r, ϕ are distance measures; $u^0, u^1 \in \mathbb{R}^N$ are background and foreground intensities; and φ is a μ-Lipschitz differentiable function. Special cases of the problem (2) include:

- The Chan-Vese case with known constants [6, 22] : φ_0, φ_1 are identity, $\nu = 0$, $u_1^0 = u_2^0 = \ldots = u_N^0$, $u_1^1 = u_2^1 = \ldots = u_N^1$, ϕ takes a quadratic form, $R = 2$, ψ_2 is the total variation penalization [23] (i.e., $P_2 = 2N$, $V_2 = \left[(\Delta^{\mathrm{h}})^\top\ (\Delta^{\mathrm{v}})^\top\right]^\top$, where $\Delta^{\mathrm{h}} \in \mathbb{R}^{N \times N}$ (resp. $\Delta^{\mathrm{v}} \in \mathbb{R}^{N \times N}$) corresponds to a horizontal (resp. vertical) gradient operator, and, for every $x \in \mathbb{R}^N$, $\psi_2(V_2 x) = \sum_{n=1}^{N} \left(([\Delta^{\mathrm{h}} x]_n)^2 + ([\Delta^{\mathrm{v}} x]_n)^2\right)^{1/2}$).
- The two phase case of wavelet frame image segmentation [8]: φ_0, φ_1 are ℓ_1 norms, $\nu = 0$, $u_1^0 = u_2^0 = \ldots = u_N^0$, $u_1^1 = u_2^1 = \ldots = u_N^1$, ϕ takes a quadratic form, $\forall r = 2, \ldots, R$, ψ_r is ℓ_1 norm and V_r is a frame operator.
- The two phase case of fuzzy segmentation [19]: φ_0, φ_1 are ℓ_2 norms, $\nu = 0$, for all $i = 1, \ldots, N$ u_i^0 (resp. u_i^1) is given by non-local mean of $\phi(y_i - u_0^i)$ (resp. $\phi(y_i - u_1^i)$) with weights defined by current estimate of x_i (resp. $(1 - x_i)$), ϕ takes a quadratic form, $R = 2$, ψ_2 is a non-convex regularization term given by $\sum_{i=1}^{N} \sum_{j \in \mathcal{N}_i} x_i(1 - x_j)$ where $\mathcal{N}_i$ denotes some local neighbourhood around pixel i.
- The two phase case of multiple piecewise constant model [18]: φ_0, φ_1 are identity, $\nu = 0$, for all $i = 1, \ldots, N$ u_i^0 (resp. u_i^1) is obtained as a result of k-means region clustering, ϕ takes a quadratic form, $R = 2$, ψ_2 is the total variation penalization [23].

In the remainder of this paper, we assume, for all $r \in \{0, \ldots, R\}$ that[1] $\psi_r \in \Gamma_0(\mathbb{R}^{P_r})$ and $\varphi \in \Gamma_0(\mathbb{R}^{P_\varphi})$.

3. PROPOSED NON-LOCAL MODEL

We consider an image x to be sparse if the foreground objects cover only a small portion of its entire support, i.e. $\delta = \frac{|\mathbb{X}_1|}{|\mathbb{X}|} \ll 1$. Images x and y are realizations of random variables X and Y, respectively.

We propose to decompose an observed image y into a set of overlapping regions centered on pixels i. Let Θ be a patch selection operator with some predefined boundary conditions, and let $\Theta y = \{\Theta y_1, \ldots, \Theta y_N\}$ be realizations of random variables $\{Y_1, \ldots, Y_N\}$. The linear operator Θ needs to be chosen such that there is a low probability that Θy_i is associated only with foreground, i.e., in each column of Θ, there is δN non zero coefficients. Under the following assumptions:

(i) δ is known;

(ii) the local ordering relationship between foreground and background is known and unchanged within the whole image;

[1] See for instance [24], that $\Gamma_0(\mathbb{R}^N)$ is the class of lower-semicontinuous, proper, convex functions from $\mathbb{R}^N$ to $(-\infty, +\infty]$.

(iii) noise is described by some symmetric probability distribution, possibly spatially variant;

we determine local values of u^1 and u^0 at each point along the image domain. More precisely, $\forall i \in \mathbb{X}$, u_i^0 and u_i^1 are set as $1-\delta$ and δ quantiles of Y_i if background is locally lighter than foreground, and as δ and $1-\delta$ quantiles of Y_i otherwise. For instance, in the latter case, we have

$$u_i^0 = \underset{q\in\mathbb{R}}{\operatorname{argmin}} \Pr\left[Y_i < q\right] \leq \delta \tag{7}$$

$$u_i^1 = \underset{q\in\mathbb{R}}{\operatorname{argmin}} \Pr\left[Y_i < q\right] \leq (1-\delta) \tag{8}$$

Note that if Θ is defined such that the target signal is distributed uniformly across the patches, all the values u_i^0 and u_i^1 are likely to describe the local intensity of the background and foreground, respectively. However, if the patch related to Y_i includes only the background (resp. the foreground) signal, the values u_i^0 and u_i^1 are chosen such that the data fidelity penalty for assigning the given pixel i to the background or to the foreground is the same. In such a case, the equal penalization is a direct consequence of the noise distribution symmetry assumption.

We propose to combine the proposed data fidelity term (Eq. (4)) with an image sparsity prior. In the context of convex optimization framework, the sparsity is usually imposed by the ℓ_1 norm. Thus we have $R \geq 2$, V_2 given by identity, and $\psi_2(x) = \lambda_2|x|$, where $\lambda_2 \in \mathbb{R}^+$ is a positive weight.

Thus, a pixel i associated with a patch including either only the background or the foreground is more likely to be assigned to the background (x_i is close to 0). Note that if the size of the patches is not well chosen, i.e., some patches include only the foreground, the signal can only be found by relying on some additional prior related to the nature of searched object, e.g., regularity, connectivity or tubularity.

4. OPTIMISATION APPROACH

The optimisation problem of Eq. (2), where f takes the form of Eq. (3), can be efficiently addressed using various convex optimizations tools, as proximal splitting algorithms (see [25] for a survey). In such framework, the solution is obtained iteratively by incorporating the function either via a proximity operator or via its gradient. Incorporating a function via proximity operator is computationally efficient provided that the explicit form of this operator exists.

Definition 1 *Let $\psi \in \Gamma_0(\mathbb{R}^N)$. For every $x \in \mathbb{R}^N$, the minimization problem consisting of finding*

$$\min_{y\in\mathbb{R}^N} \psi(y) + \frac{1}{2}\|x-y\|^2 \tag{9}$$

admits a unique solution, which is denoted by $\operatorname{prox}_\psi(x)$. The so-defined operator $\operatorname{prox}_\psi \colon \mathbb{R}^N \to \mathbb{R}^N$ is the proximity operator *of ψ.*

Hereafter, we present the general primal-dual splitting algorithm, proposed in [26] and summarized in Alg. 1, where V_0 and V_1 are identity matrices. The convergence of Alg. 1 is guaranteed by the result presented in Prop. 1, deduced from [26, Th. 4.2].

The generality of Alg. 1 stems from the fact that it allows us to solve Eq. (2) for any Lipschitz differentiable function φ and arbitrary linear operators $(V_r)_{2\leq r\leq R}$. Consequently, a wide range of penalization strategies are applicable, among them some were already studied in the context of tubular segmentation problem [23, 8, 9, 10].

Algorithm 1 Primal-dual algorithm for solving Eq. (2)

Let $\gamma \in (0,+\infty)$, $u_0 \in \mathbb{R}^N$ and $u_1 \in \mathbb{R}^N$.
Set $x_0 \in \mathbb{R}^N$, and $\forall r \in \{0,\dots,R\}$, $v_{r,0} \in \mathbb{R}^{P_r}$.
For $k = 0, \dots$
- $y_{1,k} = x_k - \gamma\left(\nabla\varphi(x_k) + \sum_{r=0}^R V_r^\top v_{r,k}\right)$
- $p_{1,k} = \operatorname{prox}_{\gamma\iota_{\mathcal{X}}}(y_{1,k})$
- For $r = 0, \dots, R$
  - $y_{2,r,k} = v_{r,k} + \gamma V_r x_k$
  - $p_{2,r,k} = \operatorname{prox}_{\gamma\psi_r^*}(y_{2,r,k})$
  - $q_{2,r,k} = p_{2,r,k} + \gamma V_r p_{1,k}$
  - $v_{r,k+1} = v_{r,k} - y_{2,r,k} + q_{2,r,k}$
- $q_{1,k} = p_{1,k} - \gamma\left(\nabla\varphi(p_{1,k}) + \sum_{r=0}^R V_r^\top p_{2,r,k}\right)$
- $x_{k+1} = x_k - y_{1,k} + q_{1,k}$

Proposition 1 *Given the following three assumptions:*

(i) *f is coercive, i.e., $\lim_{\|x\|\to+\infty} f(x) = +\infty$;*

(ii) *for every $r \in \{0,\dots,R\}$, ψ_r is finite valued;*

(iii) *$\gamma \in [\epsilon, (1-\epsilon)/\beta]$ where $\epsilon \in (0, 1/(\beta+1))$ and $\beta = \mu + \sqrt{\sum_{r=0}^R \|V_r\|^2}$;*

there exists a solution $\overline{x}$ of Eq. (2) such that the sequences $(x_k)_{k\in\mathbb{N}}$ and $(p_{1,k})_{k\in\mathbb{N}}$ converge to $\overline{x}$.

Note that, for $r \geq 2$, and $z \in \mathbb{R}^N$, the required $\operatorname{prox}_{\gamma\psi_r^*}(z)$ is given by

$$\operatorname{prox}_{\gamma\psi_r^*}(z) = z - \gamma\operatorname{prox}_{\gamma^{-1}\psi_r}(\gamma^{-1}z) \tag{10}$$

while the proximity operators of the function ψ_0 (resp. ψ_1) involved in the data fidelity term can be computed easily using the property of decomposition into orthogonal basis [25]. More precisely, for $r \in \{0,1\}$ and $z \in \mathbb{R}^N$, we have

$$\operatorname{prox}_{\gamma\psi_r^*}(z) = [p_1, p_2, \dots, p_N]^\top \tag{11}$$

where

$$p_i = z_i - \gamma\phi_{i,r}\left(\operatorname{prox}_{(\gamma\phi_{i,r})^{-1}\varphi_r}\left((\gamma\phi_{i,r})^{-1} z_i - r\right) + r\right) \tag{12}$$

with $\phi_{i,r}$ equal to $\phi(y_i - u_i^1)$ and $\phi(y_i - u_i^0)$ for $r = 0$ and $r = 1$, respectively.

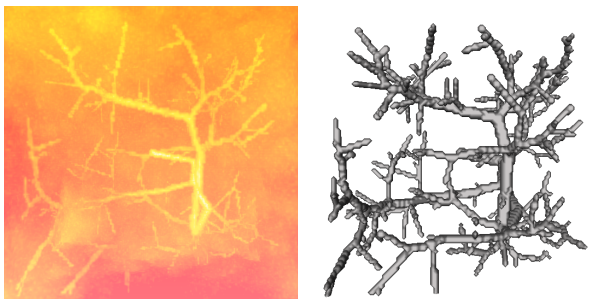

(a) Original (max. projection view) (b) Ground truth

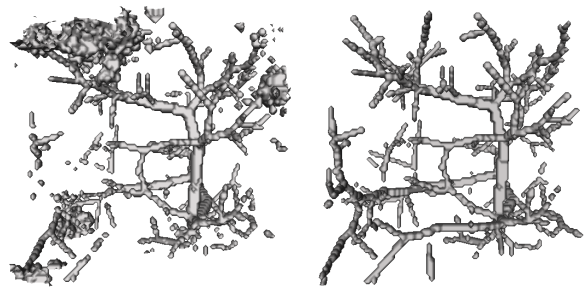

(c) Piecewise const. (0.753, 0.984) (d) Ours (0.835, 1.000)

Fig. 1. Inhomogeneous VascuSynth results (TPR, SPC).

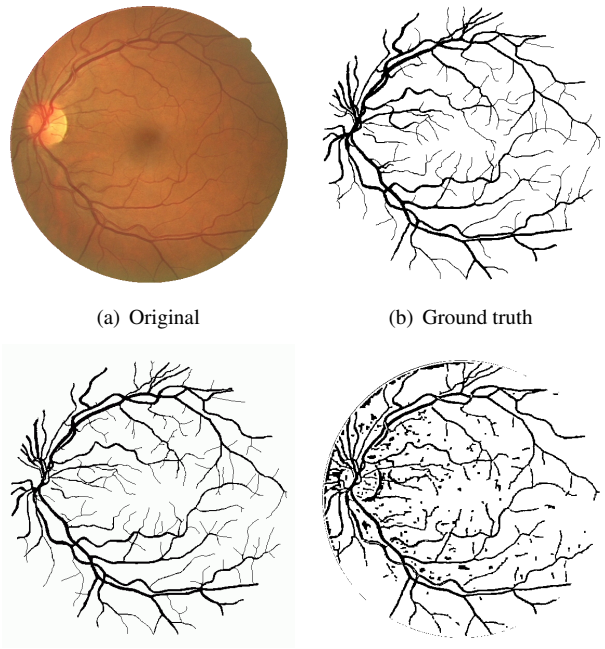

(a) Original (b) Ground truth

(c) Human (0.797, 0.972) (d) Ours (0.800, 0.936)

Fig. 2. DRIVE database visual result (TPR, SPC).

5. EXPERIMENTS AND RESULTS

We now illustrate the practical performances of our method. The segmentation involves the minimization of

$$f = \Phi + \iota_{\mathcal{X}} + \lambda_2 |\cdot| + \lambda_3 \text{ TV} + \lambda_4 \text{ H} \qquad (13)$$

where φ_0, φ_1, ϕ are defined as ℓ_1 norm, $\lambda_i > 0$ are the regularization parameters, TV and H denote the total variation and the Hessian [27, Sec. III-A] semi-norm, respectively. The quality of the results is evaluated in terms of sensitivity (TPR) and specificity (SPC). First, a study of the influence of the data fidelity choice in terms of segmentation quality is presented, i.e., we compare our non-local with classical piecewise constant model using synthetic data. Next, our method is compared to several methods from the DRIVE database [28].

In our first experiment, we use an image of size $100 \times 100 \times 100$ generated by VascuSynth [29, 30]. To generate the observed image y (Fig. 1(a)), we have introduced inhomogeneity of foreground, i.e., intensity of target signal is a function of diameter of the associated tubular structure. The image of average intensity 0.1 was further corrupted with a biased additive Gaussian random field of mean 0.2 and spatial variance 0.025, to reproduce significant background inhomogeneities and zero-mean additive Gaussian noise with $\sigma^2 = 0.05$. One can observe (Fig. 1(c), $u_0 = 0.085$, $u_1 = 0.18$, $u_0 = 0.165$, $\lambda_2 = 0.5$, $\lambda_3 = 0.025$, $\lambda_4 = 0.025$) that many poorly contrasted structures are lost using a piecewise constant model, while our method (Fig. 1(d), $\delta = 0.1$, patch size 7×7, $\lambda_2 = 0.0125$, $\lambda_3 = 0.025$, $\lambda_4 = 0.025$) preserves all structures. This is confirmed by inspecting the associated TPR and SPC values of 0.835 and 1.000, respectively.

For real data, we use images from the DRIVE database (mono channel version). The algorithm is defined by $y \in [0,1]^N$, $\delta = 0.15$, patch size 19×19, $\lambda_2 = 0.003$, $\lambda_3 = 0.0125$, $\lambda_4 = 0.0012$. The results (Fig. 2(d)) indicate that TV and H priors do not promote the solutions with the tubular structures of 1 pixel diameter. There are also some isolated structures close to the image boundary. Our method remains however competitive with respect to [31, 32] (Tab. 1). Note finally, that in contrast to [28, 33], it is unsupervised.

	Human	[28]	[33]	[31]	[32]	Ours
TPR	0.780	0.719	0.679	0.709	0.715	0.725
SPC	0.972	0.977	0.980	0.949	0.976	0.925

Table 1. DRIVE database results averaged over 20 images.

6. CONCLUSION

We have proposed a variational approach for tubular segmentation problem in the presence of inhomogeneity and noise. Taking advantage of the signal sparsity in the image domain we have developed a new non-local data fidelity term. While only TV-based segmentation was presented, the proposed framework offers significant versatility. Hence, since our results were observed to produce results with some disconnected structures (Fig. 2), as future work we plan to add to formulation (13) connectivity and tubularity priors .

7. REFERENCES

[1] D. Kaba, A. G. Salazar-Gonzalez, Y. Li, X. Liu, and A. Serag, "Segmentation of retinal blood vessels using Gaussian mixture models and expectation maximisation," in *HIS*, 2013, pp. 105–112.

[2] D. L. Wilson and J. A. Noble, "An adaptive segmentation algorithm for time-of-flight MRA data," *IEEE T Med Imag*, vol. 18, pp. 938–945, 1999.

[3] C. Florin, N. Paragios, and J. Williams, "Particle filters, a quasi-Monte Carlo solution for segmentation of coronaries," in *MICCAI*, 2005, pp. 246–253.

[4] K. Allen, C. Yau, and J. A. Noble, "A recursive, stochastic vessel segmentation framework that robustly handles bifurcations," in *MIUA*, 2008.

[5] M. W. K. Law and A. C. S. Chung, "Segmentation of intracranial vessels and aneurysms in phase contrast magnetic resonance angiography using multirange filters and local variances," *IEEE T Med Imag*, vol. 22, pp. 845–859, 2013.

[6] T. Chan, S. Esedoglu, and M. Nikolova, "Algorithms for finding global minimizers of image segmentation and denoising models," *SIAM J Appl Math*, vol. 66, pp. 1632–1648, 2006.

[7] J. A. Tyrrell, E. di Tomaso, D. Fuja, R. Tong, K. Kozak, R. K. Jain, and B. Roysam, "Robust 3-D modeling of vasculature imagery using superellipsoids," *IEEE T Med Imag*, vol. 26, pp. 223–237, 2007.

[8] C. Tai, X. Zhang, and Z. Shen, "Wavelet frame based multiphase image segmentation," Tech. Rep., Princeton University, 2012.

[9] R. Rigamonti and V. Lepetit, "Accurate and efficient linear structure segmentation by leveraging ad hoc features with learned filters," in *MICCAI*, 2012, pp. 189–197.

[10] J. Stühmer, P. Schröder, and D. Cremers, "Tree shape priors with connectivity constraints using convex relaxation on general graphs," in *ICCV*, 2013.

[11] K. W. Sum and P. Y. S. Cheung, "Vessel extraction under non-uniform illumination: A level set approach," *IEEE T Bio-Med Eng*, vol. 55, pp. 358–360, 2008.

[12] F. M'hiri, N. L. T. Hoang, L. Duong, and M. Cheriet, "A new adaptive framework for tubular structures segmentation in X-ray angiography," in *ISSPA*, 2012, pp. 496–500.

[13] M. Holtzman-Gazit, R. Kimmel, N. Peled, and D. Goldsher, "Segmentation of thin structures in volumetric medical images," *IEEE T Imag Proc*, vol. 15, pp. 354–363, 2006.

[14] J. Mille and L. D. Cohen, "3D CTA image segmentation with a generalized cylinder-based tree model," in *ISBI*, 2010, pp. 1045–1048.

[15] A. Gooya, H. Liao, K. Matsumiya, K. Masamune, and T. Dohi, "Effective statistical edge integration using a flux maximizing scheme for volumetric vascular segmentation in MRA," in *IPMI*, 2007, pp. 86–97.

[16] N. Y. El-Zehiry and L. Grady, "Vessel segmentation using 3D elastica regularization," in *ISBI*, 2012, pp. 1288–1291.

[17] S. Lankton and A. Tannenbaum, "Localizing region-based active contours," *IEEE T Imag Proc*, vol. 17, pp. 2029–2039, 2008.

[18] W. Tao and X.-H. Tai, "Multiple piecewise constant with geodesic active contours (MPC-GAC) framework for interactive image segmentation using graph cut optimization," *Image Vis Comp*, vol. 29, pp. 499–508, 2011.

[19] B. Caldairou, N. Passat, P. Habas, C. Studholme, and F. Rousseau, "A non-local fuzzy segmentation method: Application to brain MRI," *Pattern Recogn*, vol. 44, pp. 1916–1927, 2011.

[20] Y. Wang, Y. Xiong, L. Lv, H. Zhang, Z. Cao, and D. Zhang, "Vector-valued Chan-Vese model driven by local histogram for texture segmentation," in *ICIP*, 2010, pp. 645–648.

[21] C. Darolti, A. Mertins, C. Bodensteiner, and U. G. Hofmann, "Local region descriptors for active contours evolution," *IEEE T Imag Proc*, vol. 17, pp. 2275–2288, 2008.

[22] E. S. Brown, T. F. Chan, and X. Bresson, "Completely convex formulation of the Chan-Vese image segmentation model," *Int J Comp Vis*, vol. 98, pp. 103–121, 2012.

[23] L. I. Rudin, S. Osher, and E. Fatemi, "Nonlinear total variation based noise removal algorithms," *Physica D*, vol. 60, pp. 259–268, 1992.

[24] H. H. Bauschke and P. L. Combettes, *Convex Analysis and Monotone Operator Theory in Hilbert Spaces*, Springer, New York, 2011.

[25] P. L. Combettes and J.-C. Pesquet, "Proximal splitting methods in signal processing," in *Fixed-Point Algorithms for Inverse Problems in Science and Engineering*. 2011, pp. 185–212, Springer.

[26] P. L. Combettes and J.-C. Pesquet, "Primal-dual splitting algorithm for solving inclusions with mixtures of composite, Lipschitzian, and parallel-sum type monotone operators," *Set-Valued Anal*, vol. 20, pp. 307–330, 2012.

[27] S. Lefkimmiatis, A. Bourquard, and M. Unser, "Hessian-based norm regularization for image restoration with biomedical applications," *IEEE T Imag Proc*, vol. 21, pp. 983–995, 2012.

[28] J. Staal, M. D. Abramoff, M. Niemeijer, M. A. Viergever, and B. van Ginneken, "Ridge-based vessel segmentation in color images of the retina," *IEEE T Med Imag*, vol. 23, pp. 501–509, 2004.

[29] G. Hamarneh and P. Jassi, "VascuSynth: Simulating vascular trees for generating volumetric image data with ground-truth segmentation and tree analysis," *Comput Med Imag Grap*, vol. 34, pp. 605–616, 2010.

[30] "VascuSynth," `http://vascusynth.cs.sfu.ca/Software.html`.

[31] M. E. Martínez-Pérez, A. D. Hughes, A. V. Stanton, S. A. Thom, A. A. Bharath, and K. H. Parker, "Retinal blood vessel segmentation by means of scale-space analysis and region growing," in *MICCAI*, 1999, pp. 90–97.

[32] M. M. Fraz, S. Barman, P. Remagnino, A. Hoppe, A. Basit, B. Uyyanonvara, A. R. Rudnicka, and C. G. Owen, "An approach to localize the retinal blood vessels using bit planes and centerline detection," *Comput Meth Prog Bio*, vol. 108, pp. 600–616, 2012.

[33] M. Niemeijer, J. J. Staal, B. van Ginneken, M. Loog, and M. D. Abramoff, "Comparative study of retinal vessel segmentation methods on a new publicly available database," *SPIE Medical Imaging*, vol. 5370, pp. 648–656, 2004.